Mansouri, MB, Vivaldi, NA, Donnelly, CJ, Robinson, MA, Vanrenterghem, J and Reinbolt, JA

 Synthesis of Subject-Specific Human Balance Responses using a Task-Level Neuromuscular Control Platform

http://researchonline.ljmu.ac.uk/id/eprint/8063/

Article

Synthesis of Subject-Specific Human Balance Responses using a Task-Level Neuromuscular Control Platform

Journal:	*Transactions on Neural Systems & Rehabilitation Engineering*
Manuscript ID	TNSRE-2017-00175.R2
Manuscript Type:	Paper
Date Submitted by the Author:	n/a
Complete List of Authors:	Mansouri, Misagh; University of Pittsburgh, Vivaldi, Nicolas; University of Tennessee Donnelly, Cyril; The University of Western Australia, School of Sport Science, Exercise and Health Robinson, Mark; Liverpool John Moores University Vanrenterghem, Jos; Katholieke Universiteit Leuven Reinbolt, Jeffrey; The University of Tennessee, Biomedical Engineering
Note: The following files were submitted by the author for peer review, but cannot be converted to PDF. You must view these files (e.g. movies) online.	
task-based control of cog with contact modeling.avi Task-based control of cog and left foot control.avi Task-based control of cog and left foot with contact modeling.avi	

SCHOLARONE™
Manuscripts

Synthesis of Subject-Specific Human Balance Responses using a Task-Level Neuromuscular Control Platform

Misagh B. Mansouri, Nicolas A. Vivaldi, Cyril J. Donnelly, Mark A. Robinson, Jos Vanrenterghem
and Jeffrey A. Reinbolt

Abstract— **Many activities of daily living require a high level of neuromuscular coordination and balance control to avoid falls. Complex musculoskeletal models paired with detailed neuromuscular simulations complement experimental studies and uncover principles of coordinated and uncoordinated movements. Here, we created a closed-loop forward dynamic simulation framework that utilizes a detailed musculoskeletal model (19 degrees of freedom, and 92 Muscles) to synthesize human balance responses after support-surface perturbation. In addition, surrogate response models of task-level experimental kinematics from two healthy subjects were provided as inputs to our closed-loop simulations to inform the design of the task-level controller. The predicted muscle EMGs and the resulting synthesized subject joint angles showed good conformity with the average of experimental trials. The simulated whole-body center of mass displacements, generated from a single kinematics trial per perturbation direction, were on average, within 7 mm (anterior perturbations) and 13 mm (posterior perturbations) of experimental displacements. Our results confirmed how a complex subject-specific movement can be reconstructed by sequencing and prioritizing multiple task-level commands to achieve desired movements. By combining the multidisciplinary approaches of robotics and biomechanics, the platform demonstrated here offers great potential for studying human movement control and subject-specific outcome prediction.**

Index Terms—**Forward Dynamics Simulations, Neuromuscular Control, Task-level Controller, Surrogate Surfaces, Static Optimization, Predictive Balance Recovery Simulations, Musculoskeletal Modeling**

I. INTRODUCTION

HOW appropriate neural commands are selected to achieve a movement task in humans is an open question. Many activities of daily living such as standing, walking, and running are intrinsically unstable and require a high degree of neuromuscular coordination and balance control to avoid falls. Control of balance is even more challenging when the balance is impaired as a result of neurological or musculoskeletal disorders. Such conditions have drastic effects on the quality of life of patients and impose a great cost on the United States economy [1]. Experimental gait and balance biomechanics and motor control research have identified many aspects of individual and environmental risk factors for loss of balance and falls [2]–[4]; however, the number of fall events continues to rise each year [5], which provides significant rationale for the continued study of balance control. Predictive dynamic simulations with neuromuscular models can complement experiments and help uncover principles of human balance control by incorporating sensorimotor feedback that is otherwise absent in traditional musculoskeletal modeling approaches [6]–[9]. These simulations can provide access to different parts of the model as well as the input control signals and the output motion to enable studying human movement under different neurological and musculoskeletal conditions. However, performing such simulations has proven to be challenging as they require detailed anatomical musculoskeletal models and complex neuromuscular controllers in order to synthesize individual human limb movement.

Many biomechanical studies have used inverse kinematics and inverse dynamics approaches to study how differences observed in experimental joint angles, joint torques, and muscle activations can elucidate the clinical or biomechanical questions of human locomotion [10], [11]. The inverse method is however not sufficient for predicting new movements where the experimental recording is not available or when either the model or the neural control strategy changes during the experiment. The forward dynamics approach, on the other hand, can be used to predict a new movement by enabling changes to the input joint torques, muscle activations, or the musculoskeletal model itself through a feedback signal. There are many studies that utilized forward dynamics simulation to study human balance control using simplified biomechanical models [12]–[16]. Complex musculoskeletal models are

essential to understand the underlying neural strategies of balance control obtained from previous studies and how those results scale to the multi-body human model.

Complex musculoskeletal models also demand more advanced controllers. There has been significant progress in the field of robotics to develop complex feedback controllers that emulate human movement in humanoid robots [17]–[20]. Others have looked at utilizing bio-inspired controllers such as a spinal level stretch-reflex controller [21], [22] or at the supraspinal level [23], [24] to re-create human movements. Insights from both fields of robotics and neuroscience have also inspired biomechanics researchers to apply control methodologies and optimization to biomechanical models [20], [25], [26]. Similarly, studies have looked at how changing the musculoskeletal model parameters can affect the output of an intervention [27], [28] or a surgical procedure [29], [30]. These studies can benefit from integrating complex feedback controllers with complex neuromuscular models and experimental biomechanical data to simulate predictive human movements. Detailed musculoskeletal models alongside the neuromuscular control signals will allow "what if" studies to be formulated by changing not only the model parameters for individual subjects but also allows neural control strategies in both healthy and clinical populations.

In this paper, we integrated task-level control methodologies inspired from the robotics field with complex neuromuscular models and subject-specific biomechanical data from the biomechanics field in an open-source forward dynamics simulation platform (OpenSim/MATLAB platform) [31]. We created a closed-loop forward dynamic simulation framework that utilizes a detailed musculoskeletal model with 19 degrees of freedom and 92 muscles to synthesize two healthy subjects' balance responses after support-surface perturbation. Surrogate models of the two subjects' kinematics were used as a reference to the task-level controller to generate a subject-specific simulation. Single-leg balance recovery responses of the two subjects were synthesized by prioritizing three task-level commands. By integrating task-level control, complex musculoskeletal models, and experimental biomechanical data, the simulation platform discussed here provides an essential tool for generating predictive simulations of human movement.

II. Methods

Details of the closed-loop neuromuscular forward dynamics simulation platform (Fig. 1) that was used to synthesize subject-specific balance responses to support-surface perturbations are summarized in the following sections.

A. Musculoskeletal model and simulation

A three-dimensional (3D) musculoskeletal model with 92 muscle-tendon actuators and 19 degrees of freedom (DoF) was constructed in OpenSim v3.0 (Fig. 1, bottom right). The musculoskeletal model consisted of 10 body segments. The subtalar, ankle, and knee joints were modeled as one DoF revolute joints while hip and lumbar joints were modeled as 3

DoF ball joints. The pelvis body (free-floating base) was connected to the ground using 3 translational and 3 rotational DoFs. The foot-ground interactions were modeled using five Hunt-Crossley contact spheres on each foot and a half space on the support surface [32]. The stiffness and dissipation values were chosen based on material properties of skin surrounding the foot and steel for the force plates on the support surface [32].

The forward dynamics simulations were generated using our open-source OpenSim/MATLAB interface implemented in Simulink [31] (Fig. 1, bottom right). The inputs to the interface are either the 19 joint torque vectors for each DoF in the model or the 92 muscle activations for each muscle in the model. Given these inputs, the interface calls the Simbody dynamic engine [33] to solve the forward dynamics problem and numerically integrates model states (outputs) using MATLAB integrators (ODE 45 was used here). This facilitates access to the model states such as joint angles, joint velocities, muscle lengths and muscle velocities, at any time step of the dynamics simulation. This feature enables custom-made feedback controllers to be added to the open-loop forward dynamic pipeline in OpenSim [31].
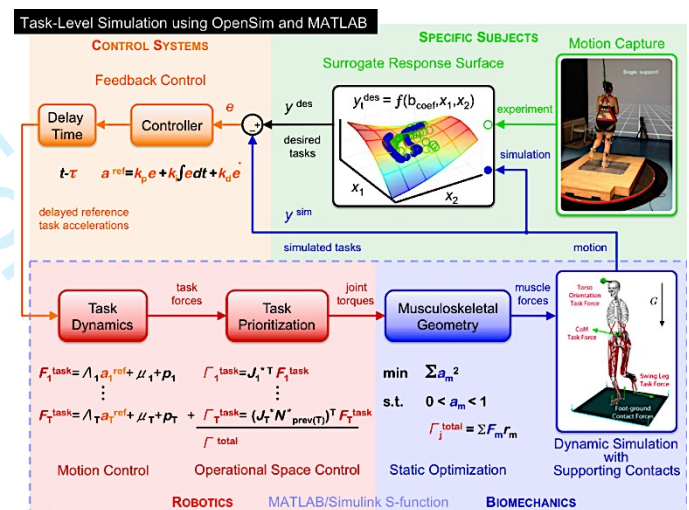

Fig. 1. Simulation framework for task-based control of movement using the experimental data. The framework consists of four major parts: the bottom right (Biomechanics), where OpenSim musculoskeletal models, forward dynamics simulations, and static optimization are used for generating a simulated subject-specific motion; the top right (Specific Subjects), where the experimental data are used to generate surrogate response surfaces representing each desired movement task; the top left (Control Systems), where the feedback tracking PID controller is used to reduce errors between desired and simulated task accelerations; the bottom left, (Robotics), where motion and operational space control are used to determine joint torques and corresponding task forces necessary for achieving the desired task-level movements.

B. Experimental setup and surrogate models of experimental movement data

We collected motion capture data (Fig. 1, top right) including

3D kinematics, ground reaction forces, and surface electromyography (sEMG) from two subjects, a female (subject1 | age 25 | height 1.72 m | mass 68 kg | foot length 26 cm) and a male (subject 2 | age 25 | height 1.79 m | mass 84.5kg | foot length 25.5 cm). The sEMG were recorded activity from 8 lower-extremity muscles (Gluteus Maximus, Gluteus Medius, Rectus Femoris, Vastus Lateralis, Vastus Medialis, Bicep Femoris, Semitendinosus, and Medial Gastrocnemius) from subjects' stance leg during single leg balance recovery experiments [29]. Muscle excitations were measured with bipolar 30 mm surface electrodes sEMG (CleartraceTM Ag/AgCl, ConMed, Utica, NY) and were recorded using a 16-channel telemetry system (Myon, Schwarzenberg, Switzerland) at 2,000 Hz sampling frequency. The raw EMGs were processed using a zero-lag fourth order Butterworth band-pass filter with the cut-off frequencies of 30 Hz to 500 Hz in MATLAB® [34]. The EMG signals were then rectified and low-pass filtered at 8 Hz to generate the linear envelope results shown in the paper. The CAREN (Computer Assisted Rehabilitation Environment) system (Motekforce Link, Amsterdam, The Netherlands) was used to introduce support-surface disturbances in the form of horizontal translations of the base of support (BoS). The CAREN platform was translated in either the anterior or posterior direction over a distance of 6 cm or 12 cm with the CAREN maximum viable working speed (40 cm/s) [35]. The subjects were instructed to maintain balance on a single leg while crossing their arms over the chest, so as not to rely on the arms for balance. Instructions given to subjects were the same for all balance recovery trials. During single-leg-support, the contralateral foot was lifted a minimum of 10 cm from the support surface. Support-surface perturbations were randomly triggered between 1 to 3 seconds after the trial had been initiated. Subjects were not given any familiarization session. The kinematics marker data was recorded and sampled at 250 Hz using VICON T40 cameras [34]. The low-pass cutoff frequency of 6 Hz was applied to the kinematics data to remove motion artifacts.

To begin forming the closed loop (Fig. 1, top right), we combined simulated biomechanical motions with subject-specific surrogate response surfaces [36], [37]. The second-order polynomial surrogate models described in equation (1) were created to represent the subjects' experimental data as task-level movement commands as follows

$$y_{\text{desired}} = b_0 + \sum_{i=1}^{2} b_i x_i + b_{12} x_1 x_2 + \sum_{i=1}^{2} b_{ii} x_i^2 \qquad (1)$$

where the response of a variable of interest (y_{desired}) is influenced by a set of predictors (x_i), and b_i are the coefficients of the second-order polynomial model for each subtask. Please refer to Appendix A for a detailed formulation of the quadratic surfaces for each subtask. Surrogate surface models were created for each subject using the subjects' kinematics responses to a single platform translation (one anterior and one posterior perturbation trial with 6 cm translations). We excluded the 12 cm platform translation trials from the surrogate models because the subjects were not able to keep their balance without stepping, which negated the single-leg

balance criterion. Separate surrogate surfaces (Fig. 1, top right) were created for each desired subtask: swing foot position (V2) (Fig. 2), torso position (V3) in x, y, and z directions as functions of the primary task, and whole-body CoM position over the base of support (V1) (Fig. 2 and Fig. 4). Previous research suggests that human dynamic stability is achieved by controlling the whole-body CoM instead of individual joint level control [38]. Consequently, the primary task was assigned to keeping the position of the whole-body CoM over the base of support. The lower-priority subtasks were then defined as controlling the swing foot position (task 2) and controlling the torso orientation (task 3). Each response surface finds a set of polynomial coefficients that best fit the subjects' experimental data. Desired tasks are computed from response surfaces as surrogate models for subject-specific motion coordination.
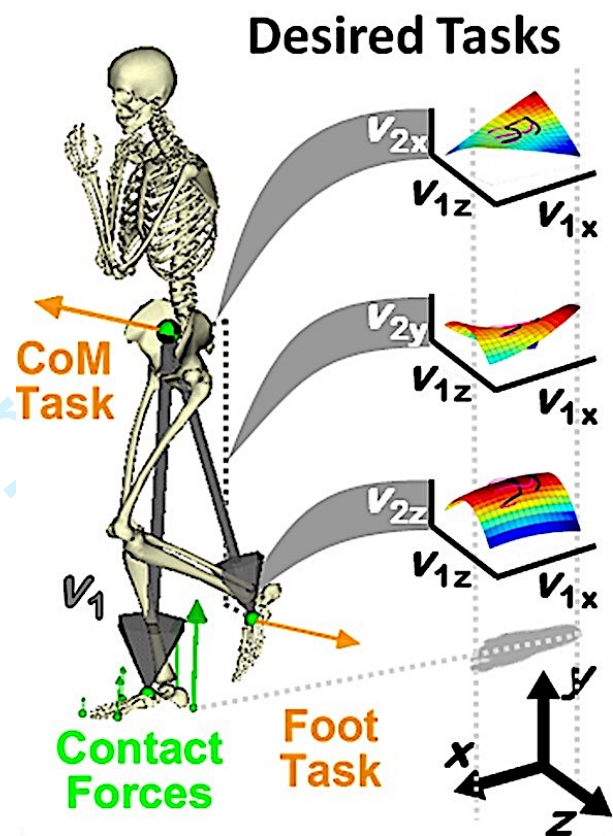

Fig. 2: Subject-specific surrogate models created from experimental motion capture data and representing desired task-level coordination. The task-level control relationships between the position of the primary task (V1), shown here as CoM task, and the swing foot position of the subtask (V2), shown here as the foot task. The third task, torso task (V3), is not shown in this figure.

C. Task-level control with task-prioritization and support-consistent contacts

We began closing the control loop with a feedback (tracking) controller for task-level commands (Fig. 1, top left). We implemented three proportional–integral–derivative (PID)

controllers that calculate the reference accelerations for each defined task using the difference between the simulated and the desired tasks positions (e.g., the simulated swing foot position compared with the experimental position on the surrogate surface). The PID gains were tuned using the PID tuner in Simulink. Similar PID gains were automatically selected for all of the tasks regardless of their priority level. This enabled us to swap different task priorities in the controller formulation with minimal need for re-tuning the PID gains. The simulated tasks (y^{sim}, Fig. 1, top right) are the 3D vector of each defined task position calculated at each simulation time step. The desired tasks ($y^{desired}$, Fig. 1, top right) are the experimental relationships of the tasks mapped to the surrogate response surfaces. The PID outputs (task accelerations) were delayed in time by a constant ($\tau = 60\ ms$) [39], [40] to represent the neuro-mechanical time lag for neural processing and neural signal transmission delays.

The delayed task accelerations calculated through the control system block (Fig. 1, top left) along with the task dynamics are used to determine the task forces required for motion control of each task (Fig. 1, bottom left). The three task forces (F^{task}) are related to the musculoskeletal model generalized torques (τ) through the multibody system Jacobian (J). The joint-space dynamics equations of motion, mass matrix (M), centrifugal and Coriolis forces (b), gravitational forces (g), were mapped into the operational space using the following equations:

$$M\ddot{q} + b + g = \tau \ \overset{J^T}{\to}\ F^{task} = \Lambda\ddot{x} + \mu + p \tag{2}$$

where $\bar{J}$ is the dynamically consistent generalized inverse of the system Jacobian (J), and

$$\Lambda(q) = (JM^{-1}J^T)^{-1}, \tag{3}$$

is the operational space mass matrix of joint space mass matrix M, and

$$\mu(q,\dot{q}) = \Lambda J M^{-1} b - \Lambda \dot{J}\dot{q} \tag{4}$$

is the operational space centrifugal and Coriolis vector, and

$$p(q) = \Lambda J M^{-1} g \tag{5}$$

is the operational space gravity vector. We utilized a support-consistent dynamics formulation derived from the robotics literature [41] with foot-ground contact modeling in OpenSim. This enabled our models to detach completely from the ground without requiring any kinematics points or weld constraints at the foot-ground contact locations. The gravity forces exerted on the musculoskeletal models push the model to the ground. Foot-ground dynamically consistent contact modeling generates the required ground reaction forces needed to move the model in 3D space. The dynamically consistent formulation also eliminates the need for any additional forces and torques (known as residuals) at the reference body (pelvis in our model) to satisfy the consistency of the equations of motion.

Task prioritization formulation [42] was implemented to control each task simultaneously. Task prioritization guarantees that joint torques for lower-priority tasks (e.g. swing leg, hands, torso positions) are not causing accelerations that interfere with any of the higher priority tasks (whole-body CoM). These subtasks were defined because healthy individuals are able to independently control their limbs with minimal effects on their overall balance control. We implemented the task prioritization formulation [43], [44] to calculate the compound torque (Γ) which consists of the main task and the non-competing subtask torques. The lower-priority subtask torques, $\Gamma_{task(k+1)}$, are defined in the null space of the higher-priority task, $N_{task(k)}$, to avoid generating any torques which conflict with the higher-priority task as follow:

$$\Gamma = \Gamma_{task} + N^T \Gamma_{subtasks}, \tag{6}$$

and in a more detailed form for our three tasks,

$$\Gamma = \Gamma_{task(1)} + N_{task(1)}^T \left(\Gamma_{task(2)} + N_{task(2)}^T \left(\Gamma_{task(3)} \right) \right), \tag{7}$$

where $N_{task(k)}$ is defined as:

$$N_{task(k)} = I - \sum_{i=1}^{k-1} \bar{J}_{i|P(i)} J_{i|p(i)}. \tag{8}$$

where I, is the $n \times n$ identity matrix, and $\bar{J}_{i|P(i)}$ is the dynamically consistent generalized inverse of the system Jacobian ($J_{i|p(i)}$). Please refer to references [45], and chapter 6 of reference [47], for the detailed dynamics formulation.

D. Inverse-dynamics-based optimization to estimate muscle forces

The last step in our simulation platform was to estimate optimal muscle activations from the calculated joint torques (Fig. 1, bottom right). Transformation from the joint torques to muscle activations is a redundant problem because there are multiple muscles that cross each joint, and they all contribute to the overall joint torque by their moment arms. One way to estimate the muscle forces and muscle activations is to use optimization. Here, we implemented static optimization in our simulation platform to minimize the sum of muscle activations squared, $\min \sum a_m^2$, (where a_m is the activation of the muscle m), subject to the inequality conditions of $0 \le a_m \le 1$. The net muscle torques, generated by multiplying muscle forces by their moment arms, must equal the total joint torques. A total of 92 muscle activations were estimated through the static optimization algorithm. We compared the simulated muscle activities with the experimental muscle EMGs that we recorded during the balance experiment.

In closing the simulation loop (Fig. 1, bottom right), the estimated muscle activations from static optimization were used to drive the forward dynamic simulations and generate the output kinematics. We compared the simulated task-level kinematics for all three tasks generated from a single trial per perturbation direction, with the average experimental kinematics recorded from both subjects (four trials from each

subject, two trials per subject, per direction) to validate our task-level controller approach in human balance control.

E. Validation

We evaluated our kinematics analyses by quantifying the amount of error that data processing created from start to finish. The simulated marker data was put through the platform to generate a synthetic dynamic simulation motion file. An artificial noise was added to the synthetic motion to simulate marker recording errors due to skin artifacts [46]. We treated the simulated marker data as the actual motion that would have occurred *in vivo* and computed synthetic and noisy data sets to compare quantitatively how far off from the true movement the final product of the platform is while taking into account error from both motion capture and data processing. Both the synthetic and noisy motions were compared to the simulated data at each phase of processing to evaluate how much error each step contributes to the endpoint results (see the flowchart in Appendix B, Fig. B1). The final synthetic and noisy dynamic simulations produced by tracking surrogate response surfaces were evaluated based on the root mean square error in joint angles (Tables 1) and task body center of mass positions (Tables 2) from the original true movements. To compare our simulation results from the proposed platform with the actual experimental kinematics, we analyzed experimental trials of single-leg balance recovery from two subjects on the CAREN platform during anterior and posterior support-surface translations.

TABLE I
ROOT MEAN SQUARE ERROR (DEGREES)

Joint Angle	Simulated to Synthetic	Simulated to Noisy
pelvis_tilt	6.77E-07	1.04
pelvis_list	4.94E-07	0.74
pelvis_rotation	5.54E-07	0.70
hip_flexion_r	9.98E-07	1.48
hip_adduction_r	5.97E-07	0.76
knee_angle_r	9.36E-07	1.26
ankle_angle_r	1.35E-06	1.65
subtalar_angle_r	1.88E-06	2.50
hip_flexion_l	8.72E-07	1.43
hip_adduction_l	6.74E-07	0.93
knee_angle_l	5.01E-07	0.78
ankle_angle_l	1.14E-06	2.63
subtalar_angle_l	1.58E-06	3.03
lumbar_extension	8.27E-07	1.16

Calculated values of the root mean square error in degrees between the simulated joint angles and those determined via inverse kinematics from the synthetic and noisy data.

TABLE II
ROOT MEAN SQUARE ERROR (METERS)

Task Position	Simulated to Synthetic	Simulated to Noisy
CoM_X	3.55E-09	4.97E-04
CoM_Y	4.10E-09	4.36E-04
CoM_Z	4.19E-09	4.86E-04
torso_X	3.98E-09	7.88E-04
torso_Y	3.81E-09	5.08E-04
torso_Z	3.20E-09	9.51E-04
calcn_left_X	4.36E-09	6.16E-04
calcn_left_Y	5.22E-09	8.00E-04
calcn_left_Z	4.03E-09	9.41E-04

Calculated values of the root mean square error in meters between the simulated whole-body center of mass, and the mass centers of the torso and the left calcaneus, and the corresponding locations determined via inverse kinematics from the synthetic and noisy data.

III. RESULTS

The quadratic surrogate response surfaces for each subject are illustrated in Appendix C. These surfaces (Fig. C1, Fig. C2) show the relationship among subtask vectors V2 (swing leg position, left calcaneus center of mass) and V3 (torso position, center of mass) and the projection of the primary task, V1 (whole-body CoM) over the BoS (anterior/posterior, x-direction, and medial/lateral, y-direction) for both the experimental (green) and the simulated trials (blue).

We compared the simulated primary task, whole-body CoM displacements, (Fig. 3, solid magenta line) and simulated subtasks, swing leg and torso displacements (Fig. 4, solid magenta line) with the average experimental task displacements (Fig. 3 and Fig. 4, blue dashed line) of both subjects' kinematics trials. The total number of 8 experimental trials, 4 trials per perturbation direction, two trials per subject per perturbation, anterior direction (subject 1, trials 86, 63; subject 2, trials 19, 44) and posterior direction (subject 1, trials 75, 46; subject 2, trials 31, 89), were analyzed to create the mean (Fig. 3, and Fig. 4, blue dashed line) and standard deviation (Fig. 3 and Fig. 4, blue gradient shadow) during both anterior (Fig. 3a, Fig. 4a, 4c) and posterior perturbations (Fig. 3b, Fig.4b, 4d). The simulated whole-body CoM displacements were, on average, within 7 mm (anterior) and 13 mm (posterior) Euclidian distance of experimental ones. The simulated position error for the subtasks such as swing leg position and torso orientation were within 2 cm average RMS error margin.
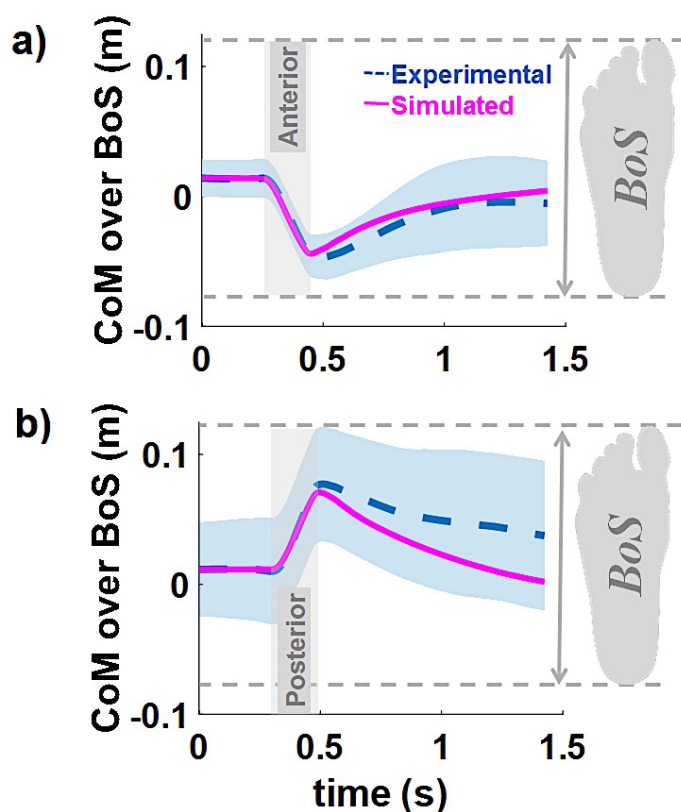
Fig. 3: Comparison of simulated (magenta, solid line) center of mass (CoM) displacement relative to the base of support (BoS) with the mean subjects' experimental CoM (blue, dash line) from four trials for each perturbation direction of both subjects (average of two trials of subject 1 and two trials of subject 2 in each direction) during a) anterior, b) posterior translation of the support surface (6 cm, 40 cm/s). The shaded blue line shows the standard deviation of the experimental data.
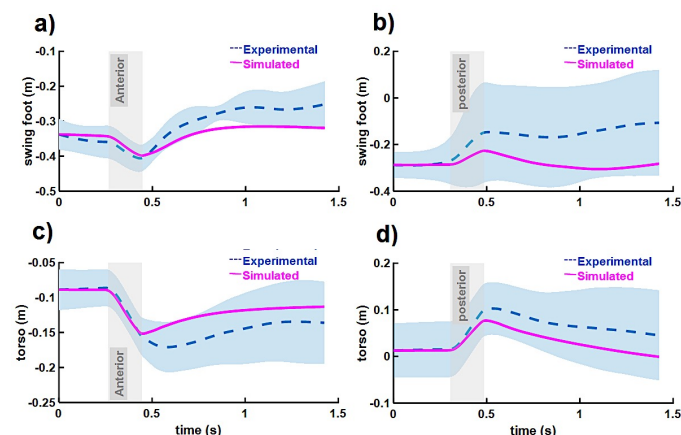

Fig. 4: Comparison of simulated subtasks-swing leg and torso positions (magenta, solid line) with the mean subjects' experimental displacements (blue, dashed line) during anterior (left column) and posterior (right column) translation of the support surface (6 cm, 40 cm/s). The shaded blue lines show the standard deviation of the experimental data.
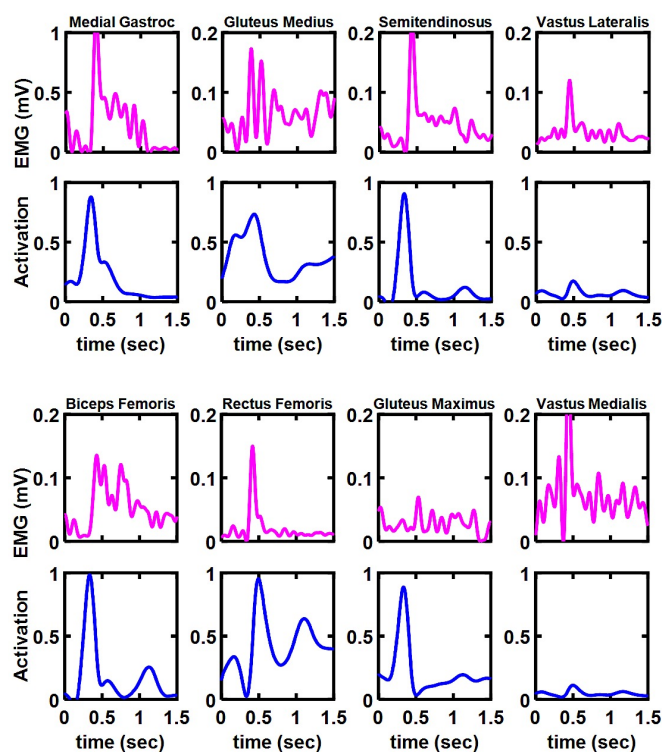

Fig. 5) Comparison of experimental (magenta) muscle EMGs (mV) and simulated (blue) muscle activations for subject 2, trial 31, during posterior perturbation (6 cm, 40 cm/s). All 8 muscle activities shown here are recorded from the subject's stance leg.

Furthermore, the comparison of the simulated muscle activities (Fig. 5, blue line) and the experimental muscle EMGs (Fig. 5, magenta line) for the 8 lower extremity muscles collected from the supporting leg of both subjects is shown here (Fig. 5, and Appendix D, Fig. D1). The simulated muscles' results show the normalized muscle activities, whereas the experimental EMG is not normalized here. Although comparison of the muscle activity magnitudes may not be relevant here, the presented results show similarities in overall EMG signal envelope shapes and contraction timings.

IV. DISCUSSION

In this paper, we merged approaches from biomechanics, control theories, and robotics in a simulation platform to enable task-level simulation of subject-specific human movement. The previously developed open-source OpenSim/MATLAB interface in Simulink [31] was utilized as a main dynamics simulation platform to provide a closed-loop task-level controller to our subject-specific detailed musculoskeletal simulations. Surrogate response surfaces were developed for each subject using a single kinematic trial to form a task-level kinematic reference that represents each subject's movement trials. The surrogate response surfaces were successful in providing high-level relationships between movement tasks required for balance control without a need for additional joint-level information. Our preliminary results showed that the

predicted results closely matched the kinematics responses from 8 kinematics trials of the two subjects for both anterior and posterior perturbations. Despite the observed task-level kinematics differences in figures 3 and 4, the overall movement patterns were analogous to the experiments by simply tracking the three task-level relationships generated from a single kinematics trial. Tracking of these task-level balance control strategies can be used to inform the design of new models that represent "typical" subjects' responses even in the situations where the experimental data is either sparse (shown in this paper) or not available. This is especially favorable for predictive simulation of human movement [30], [47], [48].

OpenSim software currently provides access to open-loop forward dynamics simulations through the "Forward Dynamics Toolbox". However, these forward simulations are however limited to fixed input signals (joint torques or muscle excitations) to solve for the estimated joint and muscle states. We used the OpenSim API's in our custom OpenSim/MATLAB interface [31] to access the musculoskeletal models' dynamic components such as mass, inertia and Jacobian matrices in MATLAB at each integration step. This enables development of custom-made controllers, such as the closed-loop task-level controller [20], [49] discussed in this paper. Combining musculoskeletal models with the neuromuscular controllers in our open-source platform allows predictive simulations to be formulated by simply providing access to modify different parts of the complex dynamic system that has not been previously available to users. These modifications can range from changing the musculoskeletal model parameters (e.g. adjusting the muscles' maximum isometric forces for different age groups, or modifying muscle-tendon attachment geometry to represent the post-surgical condition) to creating state-of-the-art controllers that represent neural control strategies (e.g. changing control parameters to generate muscle spasticity, co-contractions or other pathological conditions) in both healthy and clinical populations.

The task-level human balance control studied in this paper was inspired by previous studies which suggested similarities in high-level balance control strategies instead of individual joint-level control [50], [51]. Similarly, as discussed thoroughly in [6], previous studies suggest estimation of whole-body CoM through the integration of human sensory feedbacks (e.g., proprioceptive, vestibular and visual information) rather than joint-level information for balance control [13], [26]. Additionally, these studies demonstrate the muscles' initial burst timing and magnitude are scaled to the CoM acceleration at the onset of the perturbation [52]. Consequently, whole-body CoM was chosen as the primary task in this manuscript. The other two subtasks of swing foot and torso positions were selected to enable adequate information required for our controller to predict human balance recovery during support-surface perturbations (the supplemental videos show how the controller is able to track CoM position or swing foot through defined points using task prioritization). For our simulations,

the priority level of these subtasks can be exchanged without changing our results significantly. However, the primary task of keeping the whole-body CoM over the BoS was essential for maintaining balance; our models fell when other subtasks were selected as the primary task. In addition, despite the fact that our simulations were not sensitive to the controller PID gains, different task priority levels and gains might be necessary to compare movement across different populations (e.g. young vs. elderly subjects) or to study clinical populations such as patients with Parkinson's disease and stroke.

The results of this study should be interpreted within the context of modeling assumptions and capabilities to perform predictive simulations. In this paper, we used a single kinematics trial per perturbation direction to create reference surrogate models for two subjects' task-level balance responses to a perturbation. These surrogate models need to be expanded accordingly with additional trials to create more generalizable models that describe a specific subject population's behavioral responses to support-surface perturbations, or, expanding on our study, predicts balance under different perturbation directions and magnitudes based on a single comprehensive surrogate. The observed differences at the individual joint level between the simulated and the experimental kinematics data and consequently the observed differences in muscle activations can be meaningful depending on the clinical question that users would like to answer. Additional task-level commands (three tasks implemented in this paper) with different subtask priorities might be needed to fully represent a more complex behavioral movement and answer different specific clinical questions. Furthermore, the task-based controller can be expanded to include more physiological neural control commands and sensory feedbacks. For example, a spinal reflex model can be implemented as part of the control system using muscle spindles and Golgi tendon models [30] to encode muscle length and force feedbacks in our simulations. In addition, the static optimization technique was utilized here as a way to provide estimates of muscle activations from the joint torques. To ensure that minimization of the muscle activation is a reasonable cost function for our optimizer, the two selected trials were chosen from the trials near the middle and end of the data collection sessions (subject 1, trial 85 and subject 2, trial 31). This is in line with the previous research that showed subjects' responses to early perturbation is focused primarily on maintaining balance with little regard to the reduction of muscular effort [53] and subjects adapt their responses over the repeated perturbations. The optimization algorithm also can be modified or replaced by different cost-functions besides the energy minimization approach used here to provide a better estimate of physiological muscle EMG characteristics such as co-contraction, or muscle spasticity seen in the typical clinical population such as in stroke population. Despite these challenges, our conclusions regarding task-level simulation of human balance recovery remain valid.

The combination of detailed musculoskeletal models with the closed-loop task-level control of movement inspired by the

robotics field implemented in an open source platform [31] allowed for the synthesis of subject-specific task-level movements. We found that the quadratic surfaces can accurately predict the responses for a range of human movement data; moreover, they allow synthesis of a range of motions for a specific subject without additional prospective motion capture data (e.g., prediction of the post-treatment outcome from pre-treatment motion). Our results confirmed how a complex subject-specific movement can be reconstructed by sequencing and prioritizing multiple task-level commands to achieve a desired movement. The four areas of the closed loop (specific subjects, control systems, robotics, and biomechanics) offer numerous directions for future work to advance the study of human balance control and subject-specific outcome predictions. The novel platform presented here enables integration of task-based control with complex musculoskeletal models and has a promising outlook for integrating predictive motor control and sensory systems into the studies of human movement.

ACKNOWLEDGMENT

APPENDIX A

Form the A matrix for the primary task (V1) of a second order polynomial equation as follow:

$$A = [1; V1_X; V1_Z; V1_X{}^2; V1_X \times V1_Z; V1_Z{}^2];$$

Then compute the b coefficients for the surrogate models by solving the system of linear equations as follow for each subtask (V2, V3) in x-, y- and, z-direction,

$$b2_X = A\backslash V2_X;$$
$$b2_Y = A\backslash V2_y;$$
$$b2_z = A\backslash V2_Z;$$
$$b3_X = A\backslash V3_X;$$
$$b3_Y = A\backslash V3_Y;$$
$$b3_Z = A\backslash V3_Z;$$

and finally plug the polynomial coefficients, b, for each subtask into the second order model based on the projection of the primary task on transversal plane (support surface plane) to form the surrogate surfaces:

$$V2_X = b2_X(0) + b2_X(1) \ X + \ b2_X(2) \ Y + \ b2_X(3) \ X^2 + b2_X(4) \ XY + b2_X(5)Y^2;$$
$$V2_Y = b2_Y(0) + b2_Y(1) \ X + \ b2_Y(2) \ Y + \ b2_Y(3) \ X^2 + b2_Y(4) \ XY + b2_Y(5)Y^2;$$
$$V2_Z = b2_Z(0) + b2_Z(1) \ X + \ b2_Z(2) \ Y + \ b2_Z(3) \ X^2 + b2_Z(4) \ XY + b2_Z(5)Y^2;$$

$$V3_X = b3_X(0) + b3_X(1) \ X + \ b3_X(2) \ Y + \ b3_X(3) \ X^2 + b3_X(4) \ XY + b3_X(5)Y^2;$$
$$V3_Y = b3_Y(0) + b3_Y(1) \ X + \ b3_Y(2) \ Y + \ b3_Y(3) \ X^2 + b3_Y(4) \ XY + b3_Y(5)Y^2;$$
$$V3_Z = b3_Z(0) + b3_Z(1) \ X + \ b3_Z(2) \ Y + \ b3_Z(3) \ X^2 + b3_Z(4) \ XY + b3_Z(5)Y^2;$$
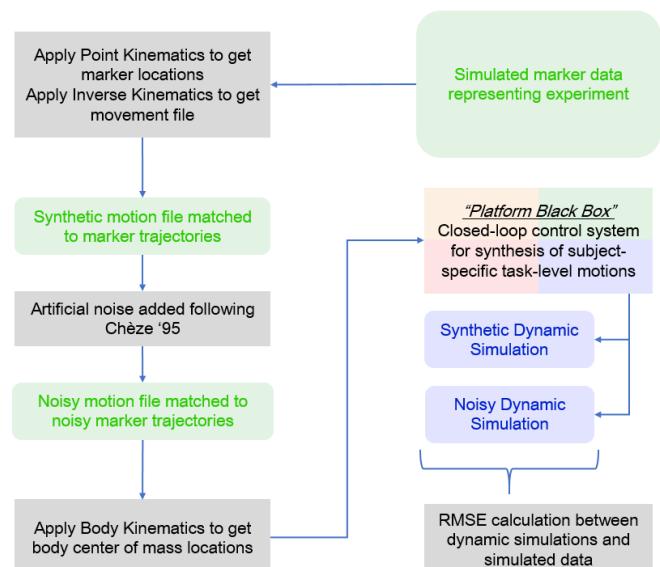
APPENDIX B

Fig. B1: Flowchart describing the steps used in validating our methods. Simulated marker data were used to represent data collection as it happens in the lab setting. Root mean square error was calculated for both synthetic and noisy fits to the simulated marker data in order to quantitatively determine the offset introduced by our modeling techniques.
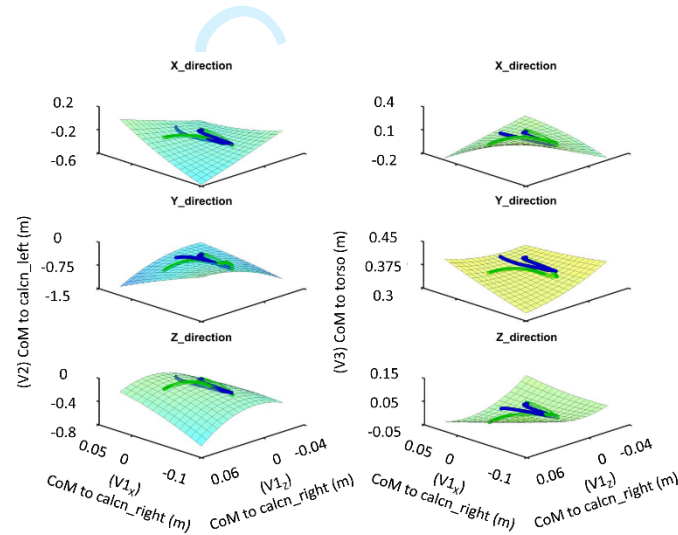
APPENDIX C

Fig. C1: Quadratic surrogate response surfaces showing the subject 2's subtasks, swing leg (left column), V2, and torso (right column), V3, over the projection of the primary task, whole-body CoM, V1, in x-, y- and, z-direction. Experimental (green) and simulated (blue). The surrogate surfaces are based on the experimental data from subject 2, trial 31.
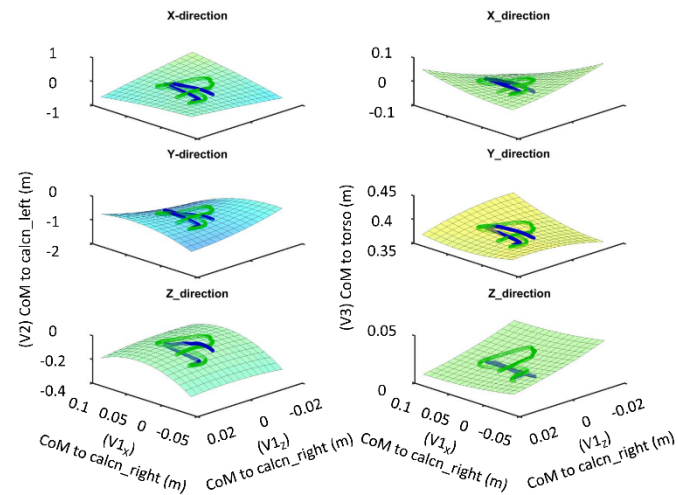

Fig. C2: Quadratic surrogate response surfaces showing the subject 1's subtasks, swing leg (left column), V2, and torso (right column), V3, over projection of the primary task, whole-body CoM, V1, in x-, y- and, z-direction. Experimental (green) and simulated (blue). The surrogate surfaces are based on the experimental data from subject 1, trial 85.
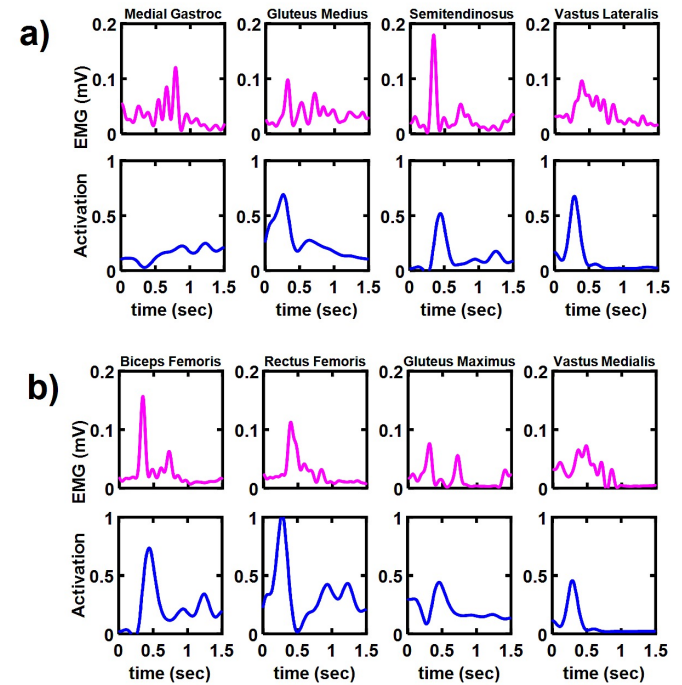
APPENDIX D

Fig. D1) Comparison of experimental (magenta) muscle EMGs (mV) and simulated (blue) muscle activations for subject 1, trial 85, during posterior perturbation (6 cm, 40 cm/s). All 8 muscle activities shown here are recorded from the subjects' stance leg.

REFERENCES

[1] C. L. Gooch, E. Pracht, and A. R. Borenstein, "The burden of neurological disease in the United States: A summary report and call to action," *Ann. Neurol.*, vol. 81, no. 4, pp. 479–484, Apr. 2017.

[2] G. E. Bertocci, M. C. Pierce, E. Deemer, F. Aguel, J. E. Janosky, and E. Vogeley, "Influence of fall height and impact surface on biomechanics of feet-first free falls in children," *Injury*, vol. 35, no. 4, pp. 417–424, 2004.

[3] M. S. Redfern *et al.*, "Biomechanics of slips," *Ergonomics*, vol. 44, no. 13, pp. 1138–1166, 2001.

[4] T. E. Lockhart, J. C. Woldstad, and J. L. Smith, "Effects of age-related gait changes on the biomechanics of slips and falls.," *Ergonomics*, vol. 46, no. 12, pp. 1136–60, Oct. 2003.

[5] CDC, "Important Facts about Falls," *Centers for Disease Control and Prevention*, 2015. [Online]. Available: http://www.cdc.gov/homeandrecreationalsafety/falls/adultfalls.html.

[6] J. L. Allen and L. H. Ting, "Why Is Neuromechanical Modeling of Balance and Locomotion So Hard?," Springer, New York, NY, 2016, pp. 197–223.

[7] F. De Groote, J. L. Allen, and L. H. Ting, "Contribution of muscle short-range stiffness to initial changes in joint kinetics and kinematics during perturbations to standing balance: A simulation study," *J. Biomech.*, vol. 55, pp. 71–77, 2017.

[8] F. Yang, F. C. Anderson, and Y. C. Pai, "Predicted threshold against backward balance loss following a slip in gait," *J. Biomech.*, vol. 41, no. 9, pp. 1823–1831, 2008.

[9] S. Piazza, M. Mansouri, D. Torricelli, J. A. Reinbolt, and J. L. Pons, "A Biomechanical Model for the Validation of Modular Control in Balance," Springer, Berlin, Heidelberg, 2013, pp. 815–819.

[10] R. A. Brindle, C. E. Milner, S. Zhang, and E. C. Fitzhugh, "Changing step width alters lower extremity biomechanics during running," *Gait Posture*, vol. 39, no. 1, pp. 124–128, 2014.

[11] K. Freyler, A. Gollhofer, R. Colin, U. Brüderlin, and R. Ritzmann, "Reactive Balance Control in Response to Perturbation in Unilateral Stance: Interaction Effects of Direction, Displacement and Velocity on Compensatory Neuromuscular and Kinematic Responses," *PLoS One*, vol. 10, no. 12, p. e0144529, Dec. 2015.

[12] R. J. Peterka, "Sensorimotor integration in human postural control.," *J. Neurophysiol.*, vol. 88, no. 3, pp. 1097–118, Sep. 2002.

[13] D. B. Lockhart and L. H. Ting, "Optimal sensorimotor transformations for balance," *Nat. Neurosci.*, vol. 10, no. 10, pp. 1329–1336, Oct. 2007.

[14] A. D. Kuo, "An optimal control model for analyzing human postural balance," *IEEE Trans. Biomed. Eng.*, vol. 42, no. 1, pp. 87–101, 1995.

[15] A. D. Kuo, "An optimal state estimation model of sensory integration in human postural balance," *J. Neural Eng.*, vol. 2, no. 3, pp. S235–S249, Sep. 2005.

[16] S. Park, F. B. Horak, and A. D. Kuo, "Postural feedback responses scale with biomechanical constraints in human standing," *Exp. Brain Res.*, vol. 154, no. 4, pp. 417–427, Feb. 2004.

[17] N. S. Pollard, J. K. Hodgins, M. J. Riley, and C. G. Atkeson, "Adapting human motion for the control of a humanoid robot," *Robot. Autom. 2002. Proceedings. ICRA '02. IEEE Int. Conf.*, vol. 2, no. May, pp. 1390–1397, 2002.

[18] B. Dariush, G. Bin Hammam, and D. Orin, "Constrained resolved acceleration control for humanoids," in *IEEE/RSJ 2010 International Conference on Intelligent Robots and Systems, IROS 2010 - Conference Proceedings*, 2010, pp. 710–717.

[19] J. Yamaguchi, E. Soga, S. Inoue, and A. Takanishi, "Development of a bipedal humanoid robot-control method of whole body cooperative dynamic biped walking," in *Proceedings 1999 IEEE International Conference on Robotics and Automation (Cat. No.99CH36288C)*, vol. 1, pp. 368–374.

[20] V. De Sapio, J. Warren, O. Khatib, and S. Delp, "Simulating the task-level control of human motion: A methodology and framework for implementation," *Vis. Comput.*, vol. 21, no. 5, pp. 289–302, 2005.

[21] H. Geyer and H. Herr, "A Muscle-Reflex Model That Encodes Principles of Legged Mechanics Produces Human Walking Dynamics and Muscle Activities," *IEEE Trans. Neural Syst. Rehabil. Eng.*, vol. 18, no. 3, pp. 263–273, Jun. 2010.

[22] H. Geyer, A. Seyfarth, and R. Blickhan, "Compliant leg behaviour explains basic dynamics of walking and running," *Proc. R. Soc. B Biol. Sci.*, vol. 273, no. 1603, pp. 2861–2867, 2006.

[23] J. L. Collinger *et al.*, "High-performance neuroprosthetic control by an individual with tetraplegia.," *Lancet (London, England)*, vol. 381, no.

9866, pp. 557–64, Feb. 2013.

[24] S. Goldfarb, D. Earl, V. De Sapio, M. Mansouri, and J. Reinbolt, "An approach and implementation for coupling neurocognitive and neuromechanical models," in *Conference Proceedings - IEEE International Conference on Systems, Man and Cybernetics*, 2014, vol. 2014–Janua, no. January, pp. 399–406.

[25] J. M. Wang, S. R. Hamner, S. L. Delp, and V. Koltun, "Optimizing locomotion controllers using biologically-based actuators and objectives," *ACM Trans. Graph.*, vol. 31, no. 4, pp. 1–11, 2012.

[26] T. D. J. Welch and L. H. Ting, "A feedback model reproduces muscle activity during human postural responses to support-surface translations.," *J. Neurophysiol.*, vol. 99, no. 2, pp. 1032–8, Feb. 2008.

[27] C. J. Donnelly, B. C. Elliott, T. L. A. Doyle, C. F. Finch, A. R. Dempsey, and D. G. Lloyd, "Changes in knee joint biomechanics following balance and technique training and a season of Australian football.," *Br. J. Sports Med.*, vol. 46, no. 13, pp. 917–22, Oct. 2012.

[28] K. D. Morgan, C. J. Donnelly, and J. A. Reinbolt, "Elevated gastrocnemius forces compensate for decreased hamstrings forces during the weight-acceptance phase of single-leg jump landing: Implications for anterior cruciate ligament injury risk," *J. Biomech.*, vol. 47, no. 13, pp. 3295–3302, 2014.

[29] J. A. Reinbolt, M. D. Fox, M. H. Schwartz, and S. L. Delp, "Predicting outcomes of rectus femoris transfer surgery," *Gait Posture*, vol. 30, no. 1, pp. 100–105, 2009.

[30] M. Mansouri, A. E. Clark, A. Seth, and J. A. Reinbolt, "Rectus femoris transfer surgery affects balance recovery in children with cerebral palsy: A computer simulation study," *Gait Posture*, vol. 43, pp. 24–30, 2016.

[31] M. Mansouri and J. A. Reinbolt, "A platform for dynamic simulation and control of movement based on OpenSim and MATLAB," *J. Biomech.*, vol. 45, no. 8, pp. 1517–1521, 2012.

[32] F. C. Anderson and M. G. Pandy, "A Dynamic Optimization Solution for Vertical Jumping in Three Dimensions," *Comput. Methods Biomech. Biomed. Engin.*, vol. 2, no. 3, pp. 201–231, Jan. 1999.

[33] M. A. Sherman, A. Seth, and S. L. Delp, "Simbody: Multibody dynamics for biomedical research," in *Procedia IUTAM*, 2011, vol. 2, pp. 241–261.

[34] C. J. Donnelly, B. C. Elliott, T. L. A. Doyle, C. F. Finch, A. R. Dempsey, and D. G. Lloyd, "Changes in muscle activation following balance and technique training and a season of Australian football," *J. Sci. Med. Sport*, vol. 18, no. 3, pp. 348–352, 2015.

[35] A. Lees, J. Vanrenterghem, G. Barton, and M. Lake, "Kinematic response characteristics of the CAREN moving platform system for use in posture and balance research," *Med. Eng. Phys.*, vol. 29, no. 5, pp. 629–635, 2007.

[36] G. E. P. Box and K. B. Wilson, "On the Experimental Attainment of Optimum Conditions," *Journal of the Royal Statistical Society. Series B (Methodological)*, vol. 13. WileyRoyal Statistical Society, pp. 1–45, 1951.

[37] J. P. Halloran, A. Erdemir, and A. J. van den Bogert, "Adaptive Surrogate Modeling for Efficient Coupling of Musculoskeletal Control and Tissue Deformation Models," *J. Biomech. Eng.*, vol. 131, no. 1, p. 11014, 2009.

[38] A. L. Hof, M. G. J. Gazendam, and W. E. Sinke, "The condition for dynamic stability," *J. Biomech.*, vol. 38, no. 1, pp. 1–8, 2005.

[39] H. Begovic, G.-Q. Zhou, T. Li, Y. Wang, and Y.-P. Zheng, "Detection of the electromechanical delay and its components during voluntary isometric contraction of the quadriceps femoris muscle.," *Front. Physiol.*, vol. 5, p. 494, 2014.

[40] S. Zhou, "Acute effect of repeated maximal isometric contraction on electromechanical delay of knee extensor muscle," *J. Electromyogr. Kinesiol.*, vol. 6, no. 2, pp. 117–127, 1996.

[41] L. Sentis and O. Khatib, "A whole-body control framework for humanoids operating in human environments," in *Proceedings - IEEE International Conference on Robotics and Automation*, 2006, vol. 2006, pp. 2641–2648.

[42] L. Sentis, "Synthesis And Control of Whole-body Behaviors in Humanoid Systems," 2007.

[43] L. Sentis and O. Khatib, "Control of free-floating humanoid robots through task prioritization," in *Proceedings - IEEE International Conference on Robotics and Automation*, 2005, vol. 2005, pp. 1718–1723.

[44] O. Khatib, "A unified approach for motion and force control of robot manipulators: The operational space formulation," *IEEE J. Robot. Autom.*, vol. 3, no. 1, pp. 43–53, 1987.

[45] M. Mansouri, "Dynamic Simulation and Neuromuscular Control of Movement: Applications for Predictive Simulations of Balance Recovery," Univeristy of Tennessee, Knoxville, 2015.

[46] L. Chèze, B. J. Fregly, and J. Dimnet, "A solidification procedure to facilitate kinematic analyses based on video system data," *J. Biomech.*, vol. 28, no. 7, pp. 879–884, 1995.

[47] L.-F. Lee and B. R. Umberger, "Generating optimal control simulations of musculoskeletal movement using OpenSim and MATLAB," *PeerJ*, vol. 4, p. e1638, 2016.

[48] C. E. Quatman, C. C. Quatman, and T. E. Hewett, "Prediction and prevention of musculoskeletal injury: a paradigm shift in methodology," *Br. J. Sports Med.*, vol. 43, no. 14, pp. 1100–1107, 2009.

[49] L. Sentis, "Synthesis and control of whole-body behaviors in humanoid systems," 2007.

[50] A. V Alexandrov, A. A. Frolov, F. B. Horak, P. Carlson-Kuhta, and S. Park, "Feedback equilibrium control during human standing.," *Biol. Cybern.*, vol. 93, no. 5, pp. 309–22, Nov. 2005.

[51] A. D. Kuo and F. E. Zajac, "Human standing posture: multi-joint movement strategies based on biomechanical constraints.," *Prog. Brain Res.*, vol. 97, no. C, pp. 349–58, Jan. 1993.

[52] T. D. J. Welch and L. H. Ting, "A Feedback Model Explains the Differential Scaling of Human Postural Responses to Perturbation Acceleration and Velocity," *J. Neurophysiol.*, vol. 101, no. 6, pp. 3294–3309, Jun. 2009.

[53] T. D. J. Welch, L. H. Ting, W. H. Coulter, and R. Balasubramaniam, "Mechanisms of Motor Adaptation in Reactive Balance Control," *PLoS One*, vol. 9, no. 5, 2014.
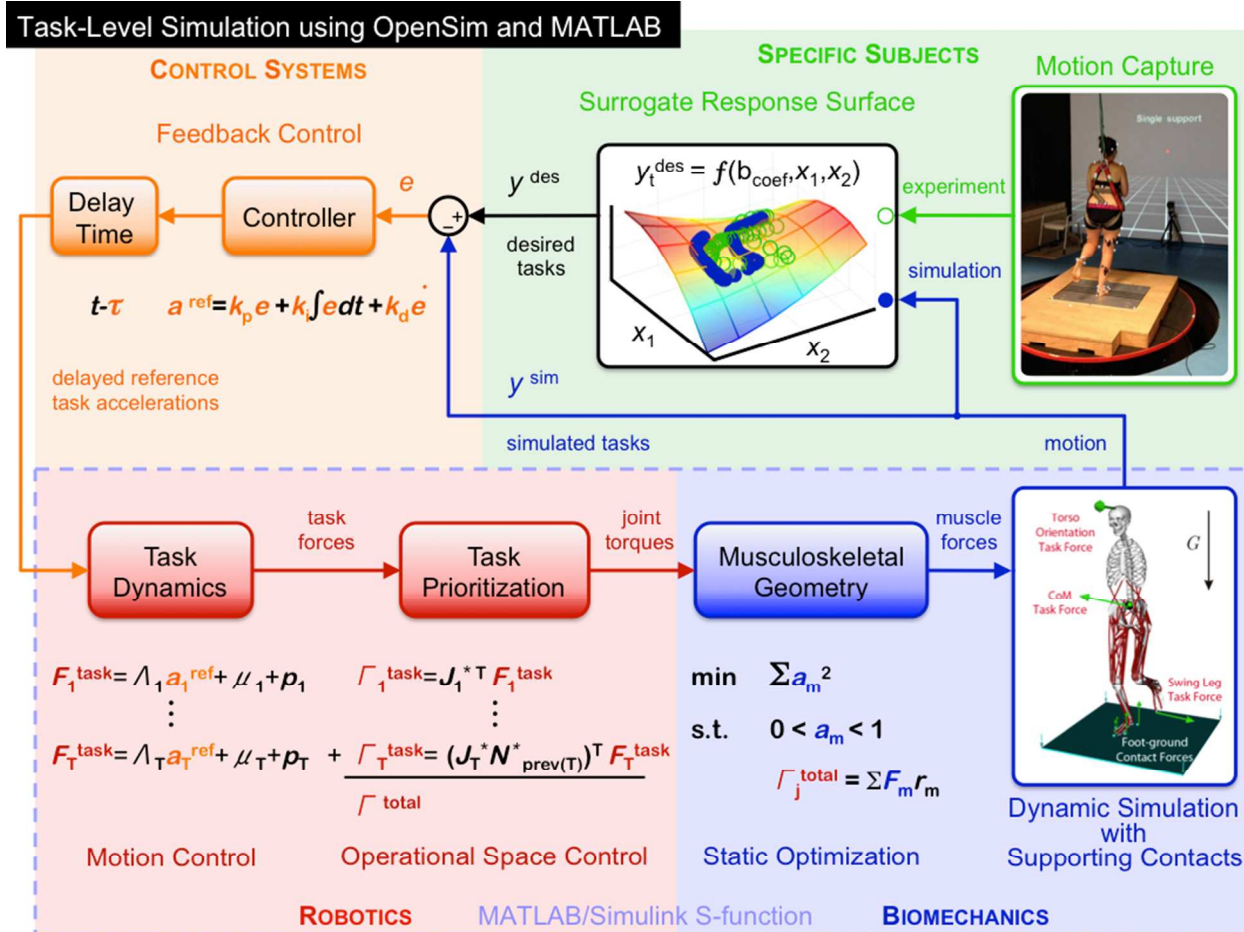
Figure 1: Simulation framework for task-based control of movement using subject-specific experimental data. The framework consists of four major parts: the bottom right (*Biomechanics*), where the OpenSim musculoskeletal modeling, forward dynamics simulations, and static optimization are used for generating a simulated subject-specific motion; the top right (*Specific Subjects*), where the experimental data are used to generate surrogate response surfaces representing each desired movement task; the top left (*Control System*s), where the feedback controller with 60 ms neuro-mechanical delay [28] is used to reduce errors between desired and simulated tasks; the bottom left (*Robotics*), where motion and operational space control are used to determine joint torques and corresponding task forces necessary for achieving the desired task-level movements.
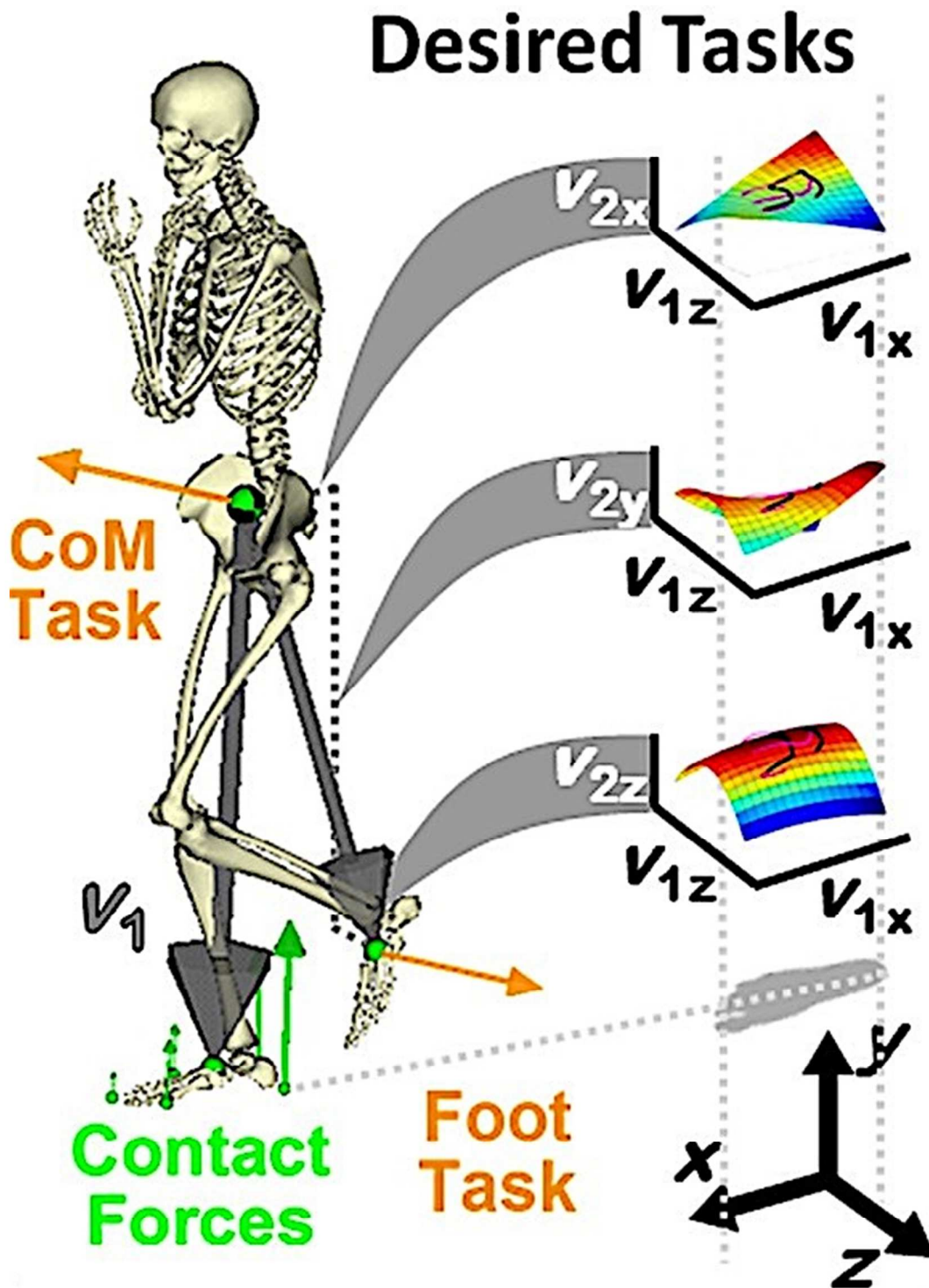
Figure 2: Subject-specific surrogate models created from experimental motion capture data and representing desired task-level coordination. The task-level control relationships between the position of the primary task (V1), shown here as CoM task, and the swing foot position of the subtask (V2), shown here as the foot task. The third task, torso task (V3), is not shown in this figure.
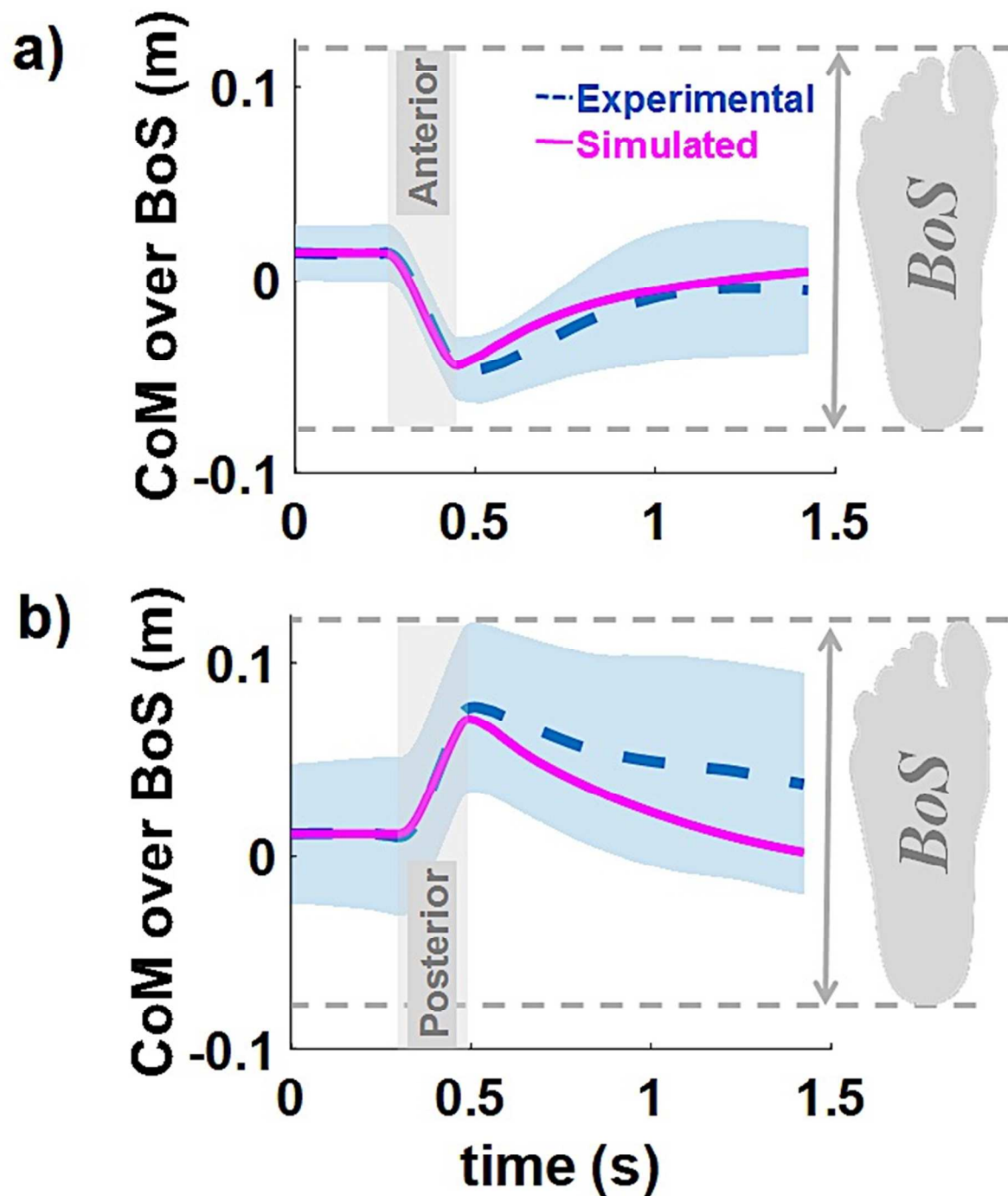
Figure 3: Comparison of simulated (magenta, solid line) center of mass (CoM) displacement relative to the base of support (BoS) with the mean subjects' experimental CoM (blue, dash line) from four trials for each perturbation direction of both subjects (average of two trials of subject 1 and two trials of subject 2 in each direction) during a) anterior, b) posterior translation of the support surface (6 cm, 40 cm/s). The shaded blue line shows the standard deviation of the experimental data.
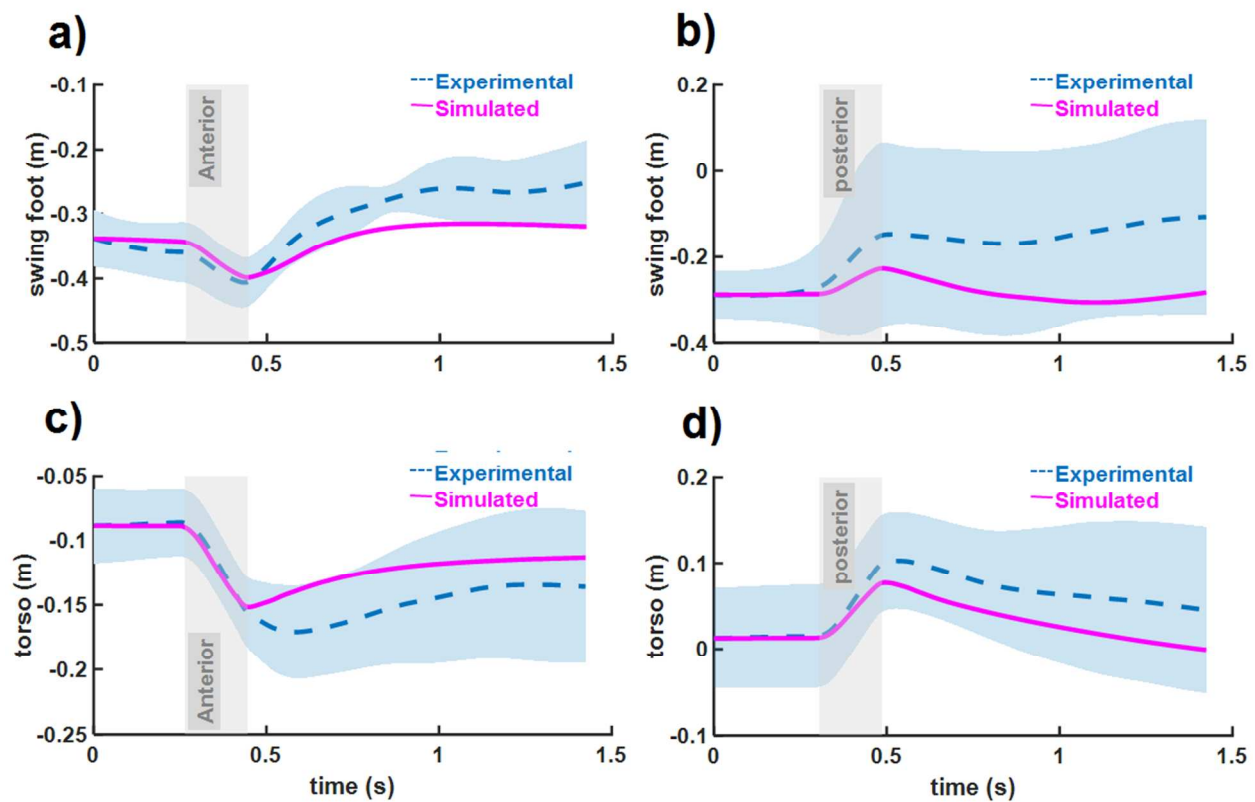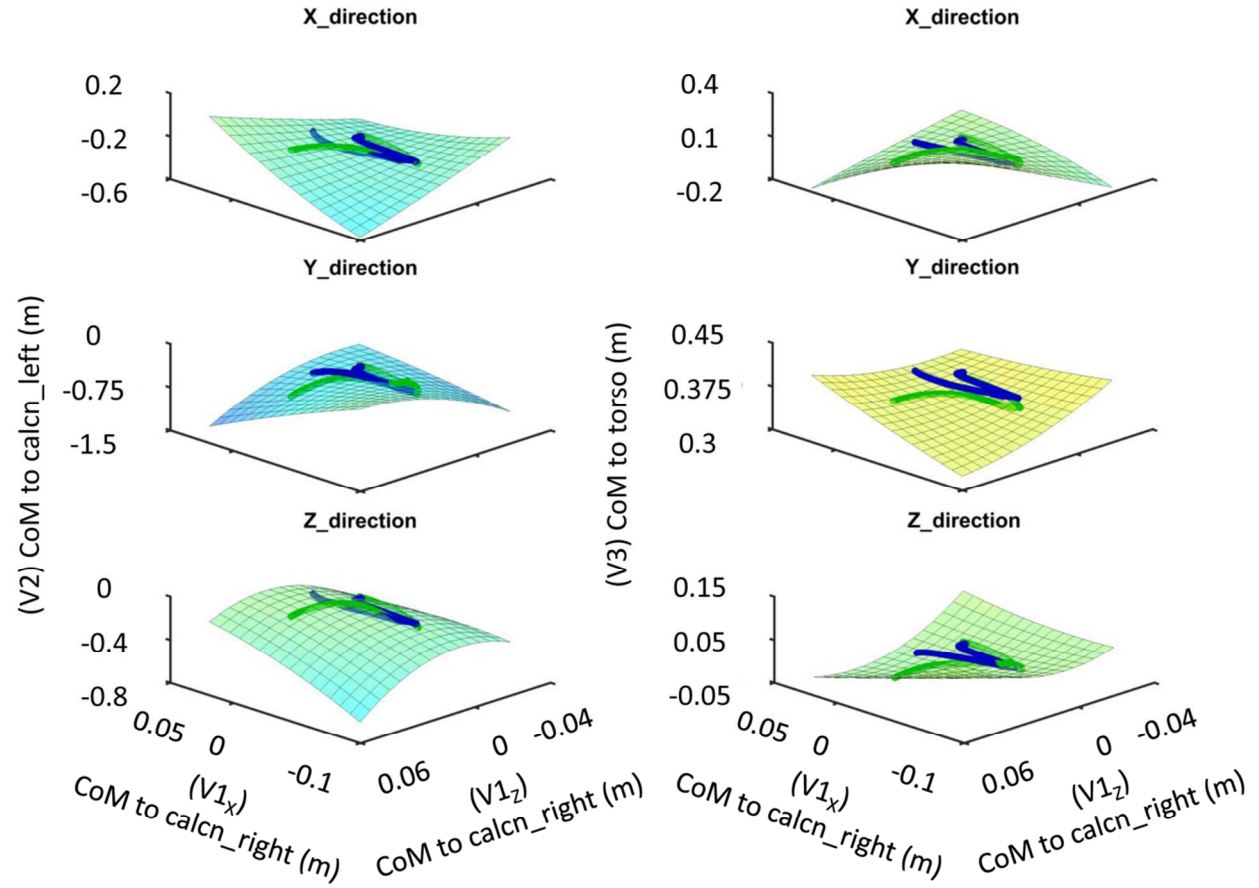
Figure 4: Comparison of simulated subtasks-swing leg and torsi positions- (magenta, solid line) with the mean subjects' experimental displacements (blue, dashed line) during anterior (left column) and posterior (right column) translation of the support surface (6 cm, 40 cm/s). The shaded blue lines show the standard deviation of the experimental data.
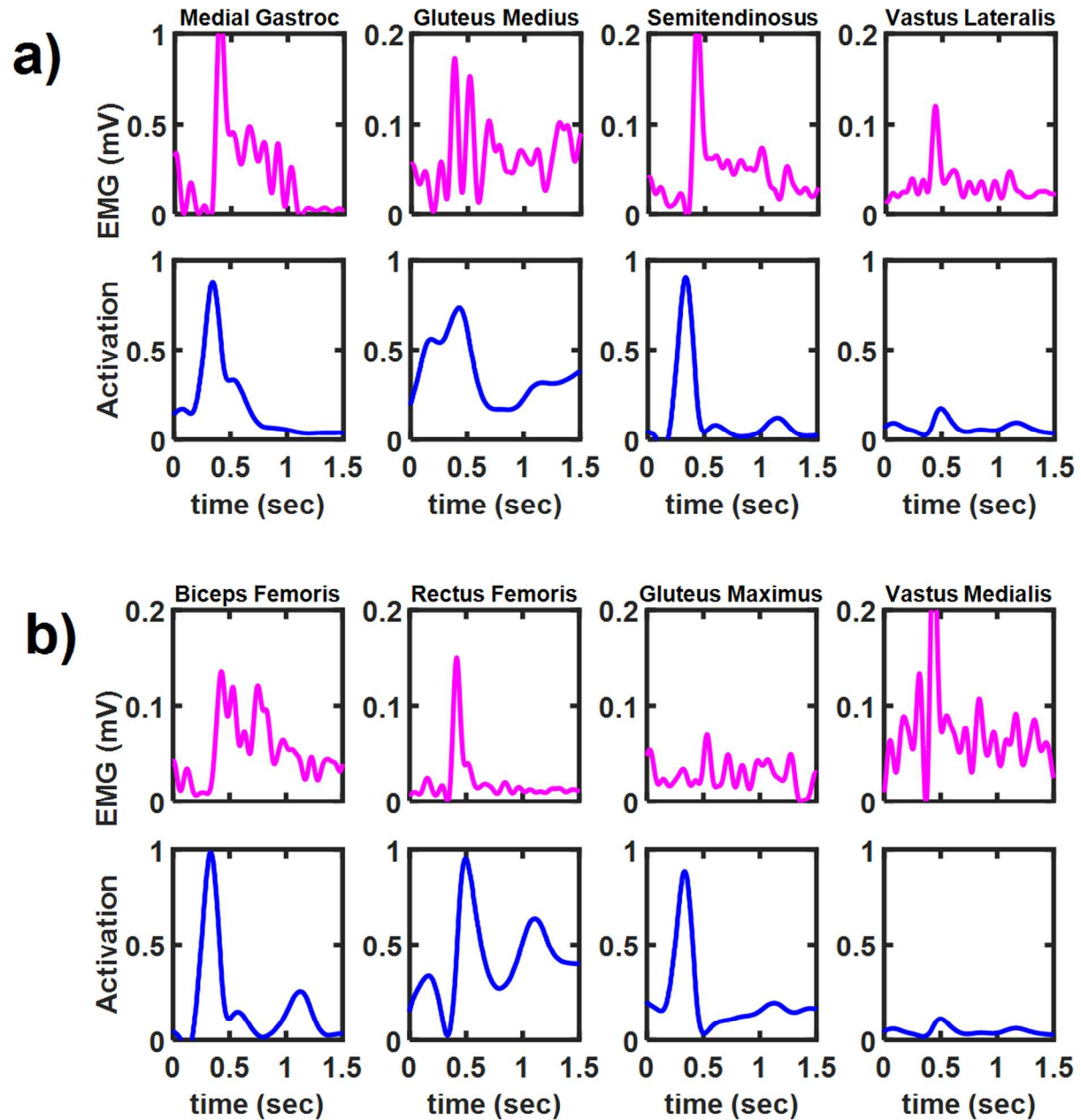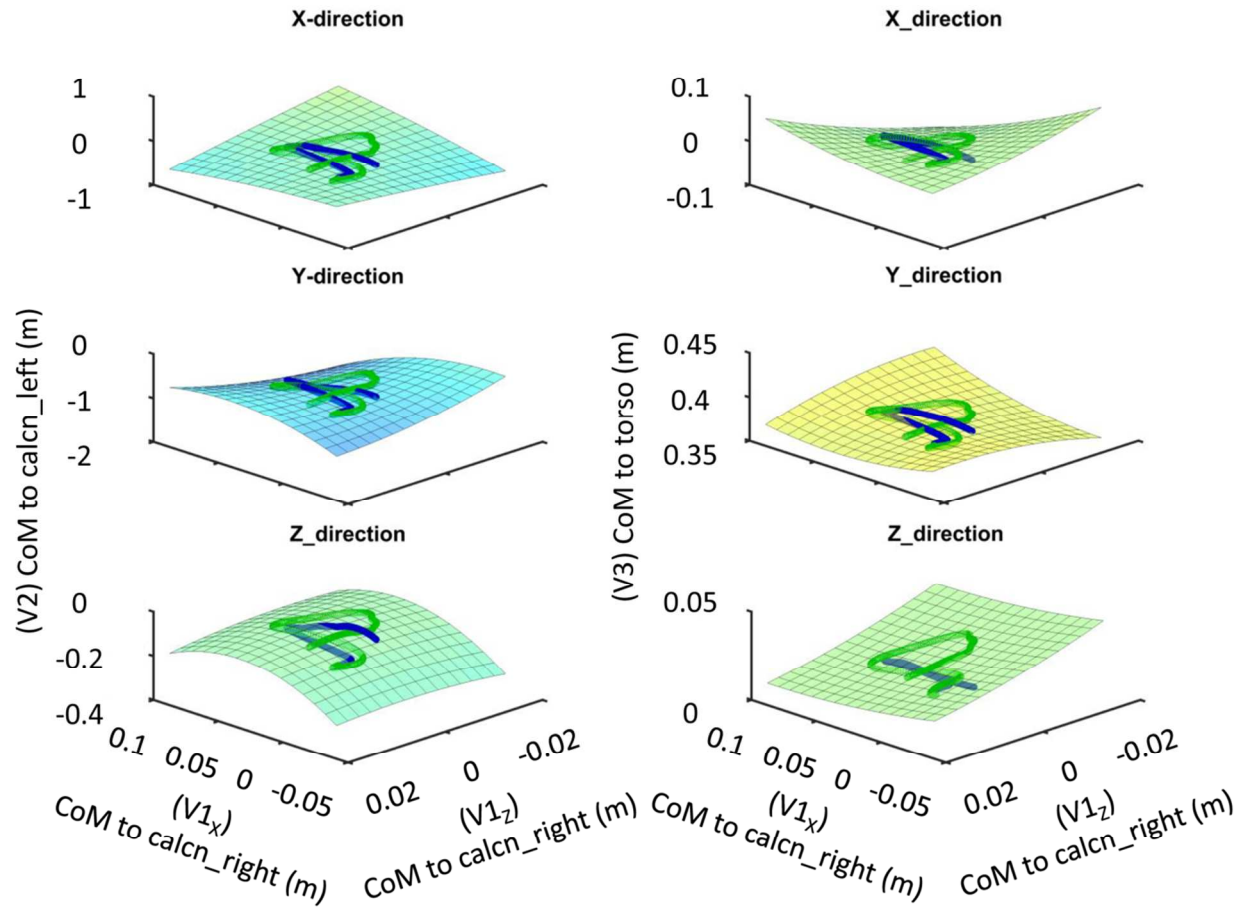
Fig. 5) Comparison of experimental (magenta) muscle EMGs (mV) and simulated (blue) muscle activations for subject 2, trial 1, during posterior perturbation (6 cm, 40 cm/s). All 8 muscle activities shown here are recorded from the subject's stance leg.
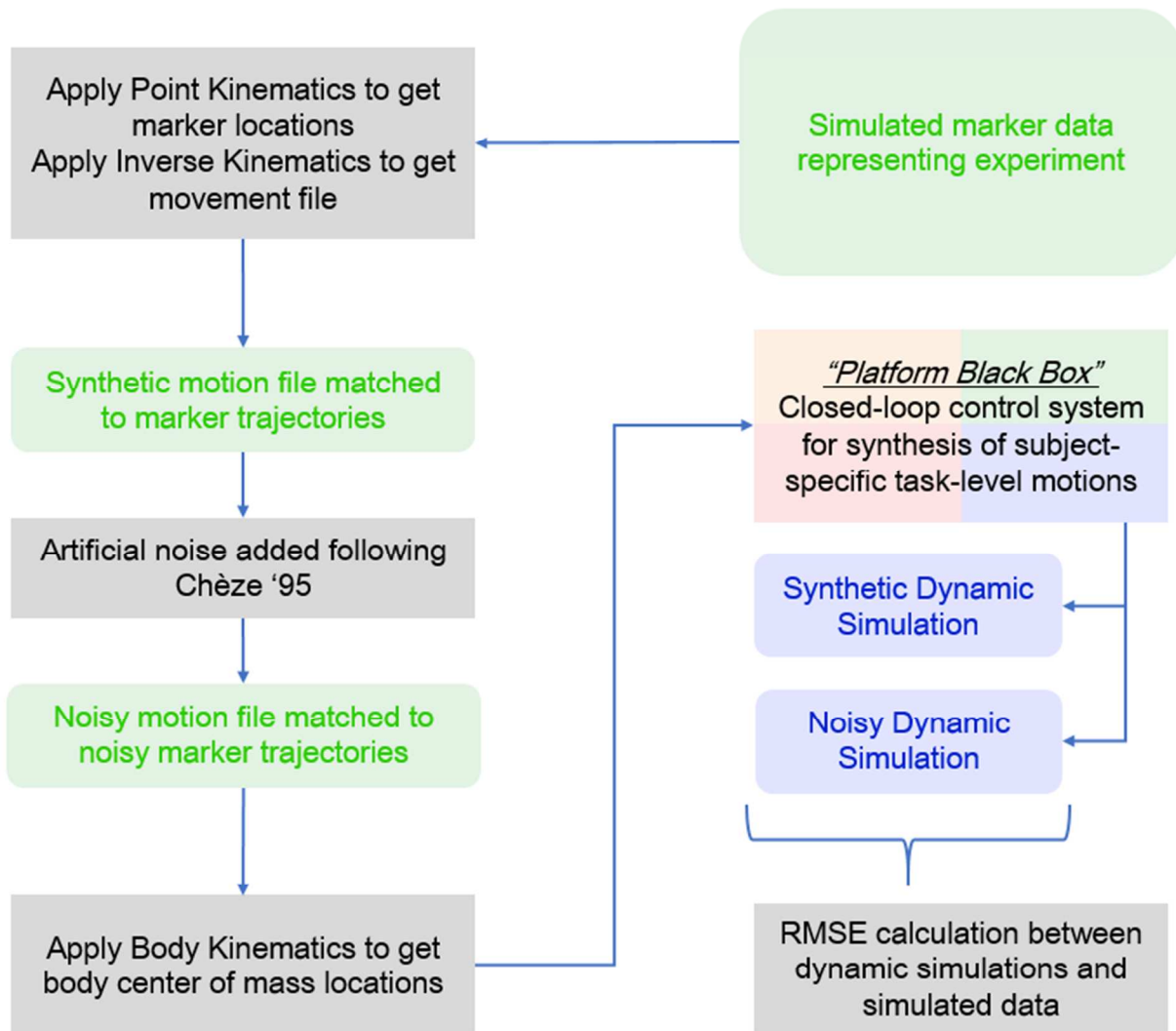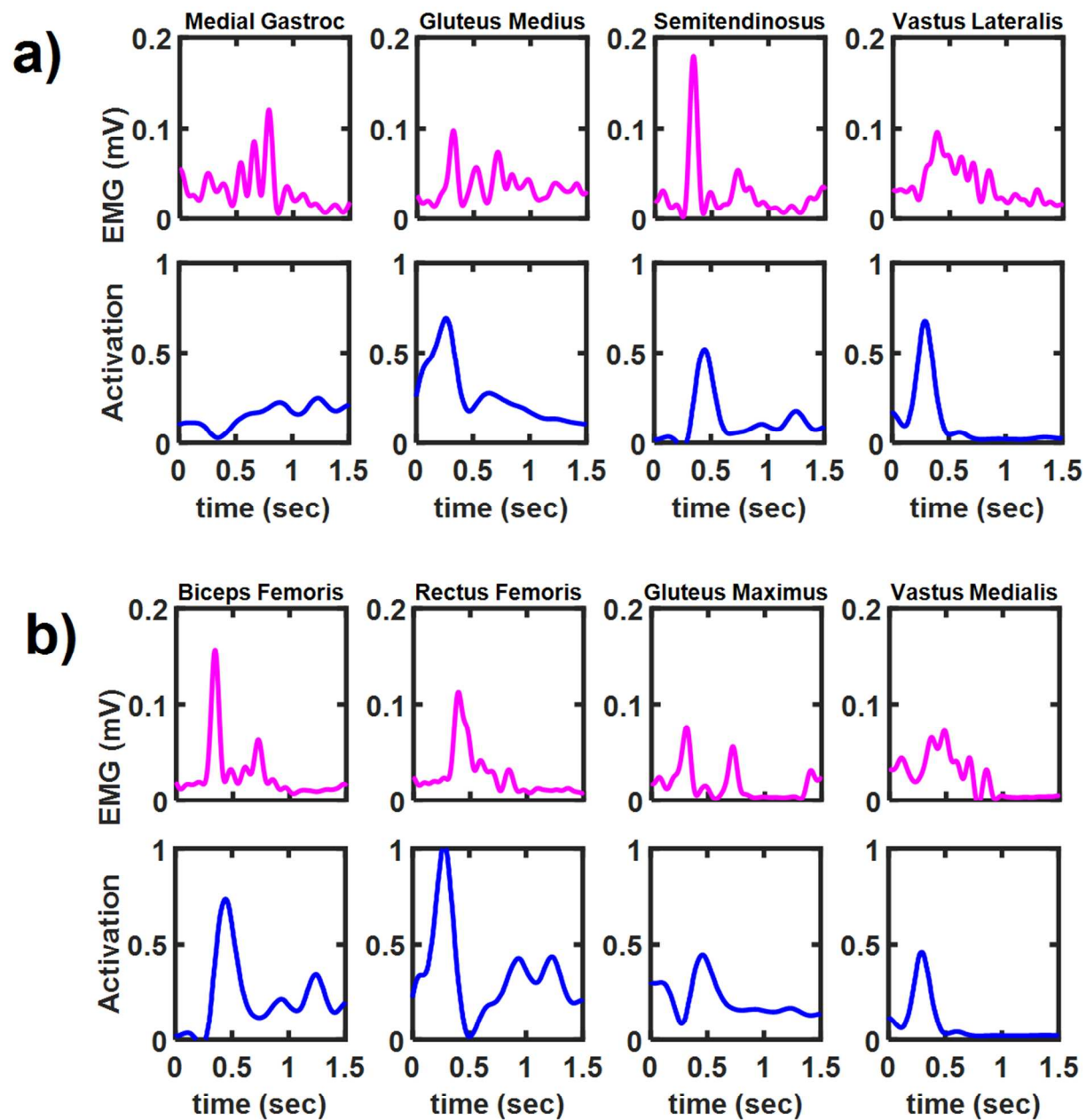
Figure B1: Flowchart describing the steps used in validating our methods. Simulated marker data was used to represent data collection as it happens in the lab setting. Root mean square error was calculated for both synthetic and noisy fits to the simulated marker data in order to quantitatively determine the offset introduced by our modeling techniques.

Fig. C1: Quadratic surrogate response surfaces showing the subject 2's subtasks, swing leg (left column), V2, and torso (right column), V3, over projection of the primary task, whole-body CoM, V1, in x, y and z direction. Experimental (green) and simulated (blue). The surrogate surfaces are based on the experimental data from subject 2, trial 31.

Fig. C2: Quadratic surrogate response surfaces showing the subject 1's subtasks, swing leg (left column), V2, and torso (right column), V3, over projection of the primary task, whole-body CoM, V1, in x, y and z direction. Experimental (green) and simulated (blue). The surrogate surfaces are based on the experimental data from subject 1, trial 85.

Fig. D1) Comparison of experimental (magenta) muscle EMGs (mV) and simulated (blue) muscle activations for subject 1, trial 85, during posterior perturbation (6 cm, 40 cm/s). All 8 muscle activities shown here are recorded from the subjects' stance leg.